The Astrophysical Journal Letters, 868:L28 (6pp), 2018 December 1 https://doi.org/10.3847/2041-8213/aaedb3

The Relation between Escape and Scattering Times of Energetic Particles in a Turbulent Magnetized Plasma: Application to Solar Flares

Frederic Effenberger[1,2] and Vahé Petrosian[3]
[1] Helmholtz Centre Potsdam, GFZ, German Research Centre for Geosciences, Potsdam, Germany; feffen@gfz-potsdam.de
[2] Bay Area Environmental Research Institute, NASA Research Park, Moffett Field, CA, USA
[3] Department of Physics and KIPAC, Stanford University, Stanford, CA, USA; vahep@stanford.edu
Received 2018 August 22; revised 2018 October 24; accepted 2018 November 1; published 2018 November 21

Abstract

A knowledge of the particle escape time from the acceleration regions of many space and astrophysical sources is of critical importance in the analysis of emission signatures produced by these particles and in the determination of the acceleration and transport mechanisms at work. This Letter addresses this general problem, in particular in solar flares, where in addition to scattering by turbulence, the magnetic field convergence from the acceleration region toward its boundaries also influences the particle escape. We test an (approximate) analytic relation between escape and scattering times, and the field convergence rate, based on the work of Malyshkin & Kulsrud, valid for both strong and weak diffusion limits and isotropic pitch-angle distributions of the injected particles, with a numerical model of particle transport. To this end, a kinetic Fokker–Planck transport model of particles is solved with a stochastic differential equation scheme, assuming different initial pitch-angle distributions. This approach enables further insights into the phase-space dynamics of the transport process, which would otherwise not be accessible. We find that in general the numerical results agree well with the analytic equation for the isotropic case; however, there are significant differences in the weak diffusion regime for non-isotopic cases, especially for distributions beamed along the magnetic field lines. The results are important in the interpretation of observations of energetic particles in solar flares and other similar space and astrophysical acceleration sites, and for the determination of acceleration-transport coefficients, commonly used in Fokker–Planck–type kinetic equations.

Key words: cosmic rays – diffusion – magnetic fields – scattering – Sun: heliosphere – Sun: particle emission

1. Introduction

The processes involved in the acceleration and transport of energetic particles in many space and astrophysical settings are still a very active topic of investigation after decades of research. These processes can be investigated by the observations of nonthermal radiations emitted from these sites and from the spectrum of cosmic rays (CRs) escaping them. Examples of these are solar eruptive events involving nonthermal radiation produced by flare-accelerated particles and solar energetic particles (SEPs) seen by near-Earth instruments. The aim of this Letter is to clarify the transport coefficients involved in the acceleration-transport processes with particular emphasis on the time the particles spend in the acceleration site, which we refer to as the escape time, $T_{\rm esc}$. We will use solar observations as an example for our discussion.

The escape time is an important component of acceleration-transport processes for several reasons. Clearly, the time spent in the acceleration site is important in shaping the energy, E, spectrum of the particles in the acceleration site, $N(E)$. It is also the main factor determining the spectrum of the flux of the escaping particles, $\dot{Q}(E) = N(E)/T_{\rm esc}(E)$. In most sources, the main transport characteristics that determine the escape time are the crossing, $\tau_{\rm cross} = L/v$, and scattering, $\tau_{\rm sc}$ (E), times, for a source of size L, and a particle with speed v. Scattering can be due to Coulomb interactions in a collisional plasma and/or wave-particle interactions in a turbulent plasma. The latter is related to the stochastic acceleration rate by turbulence or the acceleration rate in a shock environment (see, e.g., Petrosian 2012). In addition, in situations with weaker diffusion rate (i.e., when $\tau_{\rm sc}$ $(E) > \tau_{\rm cross}$ due to low particle and turbulence densities), the background guiding magnetic field, B, can affect the escape time due to mirroring in a converging field geometry. Thus, for a comprehensive analysis of particle confinement and escape from the acceleration regions, the field convergence toward the boundaries of the acceleration region needs to be considered in a particle transport model. The escape time (through its relation with $\tau_{\rm sc}$) is related to all transport coefficients so that clarifications of its role can shed light on many aspects of the acceleration process.

In general, in the acceleration process of background thermal particles (with a Maxwellian distribution), the interplay between Coulomb and turbulent scattering usually leads to plasma heating and acceleration. This can also lead to stable particle distributions consisting of quasi-thermal components with nonthermal tails, often described by kappa distributions (Bian et al. 2014), for which evidence exists from solar flare observations (Kašparová & Karlický 2009; Oka et al. 2013, 2015, 2018). As shown in Petrosian & East (2008) and Petrosian & Kang (2015), in a *closed system*, i.e., where the particle escape time is longer than all the other timescales, irrespective of the details of the acceleration process, most of the energy goes into heating the plasma rather than producing a nonthermal tail. But, when the escape time is shorter, then a substantial population of nonthermal particles can escape the acceleration site, with a spectrum that is not necessarily the same as that of the accelerated one. They are distinguished by the escape time. This distinction is important in many space and astrophysical accelerators, in particular in solar eruptive events, as described below.

A consequence of the particle interactions in the solar atmosphere is the production of thermal (due to plasma heating) and nonthermal (due to acceleration) radiation, in particular hard X-ray (HXR) bremsstrahlung, as observed for

example with the *Reuven Ramaty High Energy Solar Spectroscopic Imager* (*RHESSI*; Lin et al. 2002). The HXR observations by *RHESSI* (and earlier by *Yohkoh*) have shown the presence of a distinct source near the flaring loop top region (presumably the acceleration site) produced by the accelerated electrons. This is in addition to the more prominent footpoint emission produced by escaping electrons. (Masuda et al. 1994; Liu et al. 2008, 2013; Krucker et al. 2010), which appear to be a common feature of almost all *Yohkoh* (Petrosian et al. 2002) and *RHESSI* (Liu et al. 2006; Krucker & Lin 2008) flares. These two types of emissions are related through the escape time. Petrosian & Donaghy (1999) showed that this requires some confinement of the electrons near the loop top acceleration site, which makes the escape time longer than the crossing time, and proposed turbulence as the agent of scattering and acceleration (see also Kontar et al. 2014). Coulomb scattering can also trap particles at the loop top if the densities are high. However, because Coulomb energy loss and scattering rates are comparable, in such a case electrons lose most of their energy at the loop top leading to weaker footpoint emission. As shown by Leach & Petrosian (1983), with Coulomb collision alone one obtains a gradual decline of emission along the flaring loop with a rapid increase below the transition region. Leach & Petrosian (1983) also showed that convergence of magnetic field toward the photosphere can enhance the trapping of the particles (see their Figure 13). These effects were also discussed in Fletcher (1995) and Fletcher & Martens (1998) with similar results. They find that the confinement by the loop magnetic field can lead to a loop top emission that is stronger than or comparable to the footpoint emission for densities of 3×10^{10} (4×10^{9}) cm^{-3}; see Fletcher & Martens (1998) Figures 7 and 9, respectively.

As evident from the above discussion, observations of loop top and footpoint emissions can provide information on the escape time. The relation of HXR emission and energetic electron properties can be analyzed with forward-fitting methods or by regularized inversion using the imaging spectroscopy abilities of *RHESSI* (Piana et al. 2007). As shown by Petrosian & Chen (2010), the inversion method allows the determination of the escape time from the comparison of loop top and footpoint nonthermal electron images obtained nonparametrically from *RHESSI* data directly. Subsequently, Chen & Petrosian (2013) showed that with this technique in addition to $T_{\rm esc}$, one can obtain the other relevant coefficients (energy loss, acceleration, and crossing times). This analysis has provided a paradigm shift indicating that the mirroring effect can be the main source of confinement of particles in the acceleration site. Further evidence supporting this results comes from the interpretation by Petrosian (2016) of Krucker et al. (2007) data comparing the spectra of HXR producing and SEP electrons in impulsive, prompt events. These findings can also be useful in the interpretation of the coronal emission close to the acceleration sites in partially occulted flares (e.g., Krucker & Lin 2008; Effenberger et al. 2016, 2017), with more direct information on the acceleration process.

Magnetic field convergence and the mirroring effect can also be important in the transport of particles from coronal mass ejection (CME) shock environments. It is generally accepted that SEPs observed near the Earth are particles escaping from flare sites or the upstream region of such shocks. Recently, the *Fermi* Large Area Telescope (LAT) has detected >100 MeV sustained solar gamma-ray emission from many eruptive events (Ajello et al. 2014; Pesce-Rollins et al. 2015; Ackermann et al. 2017) associated with fast CMEs, lasting almost as long as the accompanying SEPs. These post-impulsive emissions, with no other accompanying radiative signatures, have raised the possibility that they may be produced by particles escaping the turbulent downstream region of the CME-shock back to the Sun along converging field lines (Jin et al. 2018). Thus again, analysis of these events requires a knowledge of the escape time from a region where turbulence and field geometry can play an important role.

An analytic approximation relating the escape and scattering times of particles in a converging field environment has been provided in Malyshkin & Kulsrud (2001). One of our goals is to test the validity of this relation with a numerical particle transport model and explore different initial pitch-angle distributions, in addition to the isotropic one considered by these authors.

In the next section we describe the origin of this analytic expression. In Section 3 we present the transport equations of particles in a turbulent site with simple converging field geometry, the simulation scheme that we use to determine pitch angle and spatial distributions of particles subject to only pitch-angle scattering, and address the determination of the escape time. The results are presented and discussed in Section 4, followed by the summary and conclusions in Section 5.

2. The Escape Time

As described above, several factors play an important role in trapping the particles and determining how fast particles can escape a turbulent magnetized plasma, which is the case for the particle acceleration in most astrophysical accelerators. The most important factor is the ratio of the particle scattering mean free path to the size of the source $\lambda/L \sim \tau_{\rm sc}/\tau_{\rm cross}$. In what follows we will use the pitch-angle averaged scattering time $\tau_{\rm sc} \sim \lambda/v$ and crossing time $\tau_{\rm cross} \sim L/v$, where v is the particle speed. In sources with strong guiding magnetic field, the divergence or convergence of the field described by the parameter $\eta = B_{\rm esc}/B_0$, where $B_{\rm esc}$ denotes the increased field at the boundary, and B_0 is the field strength in the center of the domain, also plays an important role. The third factor is the momentum or (for magnetized plasmas) the pitch-angle distribution. In the strong diffusion limit this ratio is small ($\tau_{\rm sc} \ll \tau_{\rm cross}$) and the particles are isotropized quickly. They are able to random walk across the source with $T_{\rm esc} \sim \tau_{\rm cross}^2/\tau_{\rm sc}$ without much effect due to magnetic field variations on the scale $h_b \equiv -B/(\partial B/\partial z \sim L \gg \lambda$. On the other hand, in the weak diffusion limit with $\tau_{\rm sc} \gg \tau_{\rm cross}$, particles move freely and escape within one crossing time unless there is a strong field convergence toward the boundary of the region, which can trap particles by mirroring. In this case the escape time is determined by how fast particles are scattered into the loss cone, in which case for an isotropic distribution $T_{\rm esc} \propto \tau_{\rm sc}$, with the proportionality constant increasing with increasing field convergence rate η. The three regimes can be summarized as

$$\frac{T_{\rm esc}}{\tau_{\rm cross}} = \begin{cases} 1 & \text{if } \tau_{\rm sc} \gg \tau_{\rm cross}, \text{ Free stream} \\ \tau_{\rm cross}/\tau_{\rm sc} & \text{if } \tau_{\rm sc} \ll \tau_{\rm cross}, \text{ Strong diffusion} \\ \propto \tau_{\rm sc}/\tau_{\rm cross} & \text{if } \tau_{\rm sc} \gg \tau_{\rm cross}, \text{ Converging field.} \end{cases}$$

The combination of the first two as $T_{\rm esc}/\tau_{\rm cross} = 1 + \tau_{\rm cross}/\tau_{\rm sc}$ is commonly used (see, e.g., Petrosian & Liu 2004)

for uniform or chaotic magnetic field situations. This can be generalized by combining with the third case to a simple analytical approximate formula relating the particle escape and scattering as (Petrosian 2016)

$$T_{\rm esc} = \tau_{\rm cross}\left[C_1(\eta) + C_2(\eta)\frac{\tau_{\rm cross}}{\tau_{\rm sc}} + C_3(\eta)\frac{\tau_{\rm sc}}{\tau_{\rm cross}}\right], \quad (1)$$

with coefficients that depend only on the value of η and on the degree of the isotropy of the distribution. The appendix in Malyshkin & Kulsrud (2001) gives an extensive discussion on these dependences leading to the following equation valid for an isotropic distribution:

$$T_{\rm esc} = \tau_{\rm cross}\left[2\eta + \frac{\tau_{\rm cross}}{\tau_{\rm sc}} + \ln\eta\frac{\tau_{\rm sc}}{\tau_{\rm cross}}\right]. \quad (2)$$

For distributions with substantial anisotropy we expect deviations from this equation, especially in the weak diffusion limit. Below we compare our simulation results with this equation.

3. Particle Transport Model with Field-line Convergence

In this section, we evaluate the effects of pitch-angle scattering and field convergence on the transport of particles through the acceleration site. For simplicity, we ignore any energy gain (often attributed to scattering by turbulence) or loss (as expected in Coulomb scattering and radiative processes) that are normally present in acceleration sites.

3.1. Transport Equation and Coefficients

To study the influence of pitch-angle scattering on the particle escape at a fixed given energy, the general Fokker–Planck equation for particle transport (e.g., Schlickeiser 1989; Armstrong et al. 2012), which is common in solar flare (e.g., Leach & Petrosian 1981; McTiernan & Petrosian 1991) and interplanetary particle transport studies (e.g., Roelof 1969; Earl 1981; Effenberger & Litvinenko 2014), can be reduced to the following energy independent form:

$$\frac{\partial f}{\partial t} + \mu v\frac{\partial f}{\partial z} + \frac{v}{2h_B}(1-\mu^2)\frac{\partial f}{\partial \mu} = \frac{\partial}{\partial \mu}\left(D_{\mu\mu}\frac{\partial f}{\partial \mu}\right), \quad (3)$$

for $f = f(z,\ \mu,\ t)$. Here, z is the distance along the mean magnetic field B, t is time, μ is the cosine of the particle pitch angle, $h_B = -B/(\partial B/\partial z)$ is the field convergence scale height, and $D_{\mu\mu}$ denotes the pitch-angle diffusion Fokker–Planck coefficient.[4]

We consider isotropic pitch-angle scattering with the diffusion coefficient

$$D_{\mu\mu} = D_0(1-\mu^2), \quad (4)$$

where D_0 is a constant which quantifies the strength of the scattering. In the diffusion approximation, which is essentially an average of the pitch-angle dependence of the particles, the respective parallel spatial diffusion coefficient along z is given by (e.g., Dung & Petrosian 1994; Schlickeiser & Shalchi 2008)

$$\kappa_{zz} = \frac{v\lambda}{3} = \frac{v^2}{8}\int_{-1}^{1} d\mu\frac{(1-\mu^2)^2}{D_{\mu\mu}} = \frac{v^2}{6D_0} \quad (5)$$

The scattering time can thus be defined as

$$\tau_{\rm sc} = \frac{\lambda}{v} = \frac{1}{2D_0}. \quad (6)$$

We normalize all quantities to the length of the system L and the particle speed v. Time is thus measured in units of $\frac{L}{v}$, while we define the ensemble crossing time as $\tau_{\rm cross} = \frac{L}{v\sqrt{2}}$, appropriate for an isotropic pitch-angle distribution.

3.2. Stochastic Simulation Scheme

Stochastic differential equations (SDEs) are used in many contexts to solve Fokker–Planck type equations. In space physics, they are often employed to solve particle propagation problems, such as CR modulation (Strauss et al. 2011; Effenberger et al. 2012), SEP transport (Dröge et al. 2010), shock acceleration (Achterberg & Schure 2011; Zuo et al. 2011), focused acceleration (Armstrong et al. 2012), and pick-up ion evolution (Fichtner et al. 1996; Chalov & Fahr 1998). For a recent account of numerical methods and other aspects connected to this approach, see, e.g., Kopp et al. (2012) and the review Strauss & Effenberger (2017). In the context of solar flares, MacKinnon & Craig (1991) presented one of the first simulation schemes based on the SDE approach. Recently, this method has also been employed in studies of the warm-target model (Jeffrey et al. 2014; Kontar et al. 2015) and coupled hydrodynamic simulations of solar flares (e.g., Moravec et al. 2016).

For our purposes, we can recast the transport Equation (3) with isotropic scattering into the following set of SDEs (e.g., Gardiner 2009)

$$dz = \mu v dt, \quad (7)$$

$$d\mu = \left[\frac{v}{2h_B}(1-\mu^2) - 2D_0\mu\right]dt + \sqrt{2D_0(1-\mu^2)}\,dW(t), \quad (8)$$

where $W(t)$ represents a Wiener process with zero mean and variance t.

Ignoring the convergence term, which can be treated separately (see below), these equations can be solved numerically using a simple Euler approximation scheme (Kloeden & Platen 1995):

$$z_{t+\Delta t} = z_t + \mu_t v\Delta t, \quad (9)$$

$$\mu_{t+\Delta t} = \mu_t - 2D_0\mu_t\Delta t + \sqrt{2D_0(1-\mu_t^2)\Delta t}\,\epsilon_t, \quad (10)$$

where ϵ_t is a normal random variable with zero mean and unit variance and Δt is a small time step (Strauss & Effenberger 2017). We use reflecting boundaries at $\mu = \pm 1$ to conserve the probability.

In practice, this system of coupled ordinary SDEs is solved numerically by following a large number of pseudo-particle orbits according to the above scheme and obtaining the distribution functions by corresponding averages over the particle positions in phase space. We can consider different initial conditions by changing the starting position of the

[4] Note that depending on the exact definition of f, the h_B dependent convergence term may be written in implicit or explicit form (e.g., Earl 1981; Litvinenko & Noble 2013). For our purposes, in the following, we will consider a simplified model of mirroring and confinement that does not require this term in the integration scheme, as described in the following sections.

particles using a suitable sampling of the initial distribution. For the purposes of this study, we will focus on three different forms of initial pitch-angle distributions: isotropic, "pancake," i.e., sharply peaked at 90° pitch angle, and beam-like, i.e., two beams of particles at $\mu = \pm 1$.

3.3. Field Convergence and Particle Escape

The two main processes in our model are pitch-angle scattering and the background magnetic field convergence or mirroring effect. The latter can be included in a straightforward way in the SDE model described above. Consider a magnetic field increase prescribed by the parameter η defined in Section 2. The loss cone of particles, i.e., the threshold pitch angle, beyond which particles escape, can be defined as $\mu_{\rm crit} = \sqrt{1 - 1/\eta}$ (Malyshkin & Kulsrud 2001).

We assume an idealized field geometry, where the effect of field convergence only applies point-wise at the boundaries of the domain. With this condition, particles are only reflected back into the domain at the boundary ($z = \pm 1$) if their pitch angle is smaller than $\mu_{\rm crit}$. Otherwise they are counted as escaped particles. Thus, for a given set of parameters, the escape time $T_{\rm esc}$ can simply be calculated as the average time the particles take to leave the domain through the loss cone. It is therefore not necessary, as mentioned before, to include the convergence term in the integration scheme explicitly, as the effect is accounted for by the selective reflection or escape of particles through the loss cone. In other words, the escape time is approximated as the ensemble average or first moment of the residence time distribution of escaping particles. In practice, the simulation runs until all particles have escaped the domain. In the upper panel of Figure 1 it can be seen how particles exit the phase-space domain at $z = \pm 1$ for μ close to ± 1.

Furthermore, Figure 1 illustrates the time evolution of the pseudo-particle ensemble and the associated phase-space distribution resulting from a hexagonal binning. In the upper panel, we consider a uniform initial pitch-angle distribution, $\eta = 2$ and a diffusion coefficient of $D_0 = 0.1$ (or $\tau_{\rm sc} = 5L/v$). We see how particles that started close to $\mu = \pm 1$ move quickly to the escape region and are not reflected back into the domain. At $t = 2$ the contribution of reflected particles with $\mu < \mu_{\rm crit}$ is visible as secondary patches in the distribution. Eventually, most of the particles will have escaped the region and this allows us to calculate the approximate escape time. The lower panel shows the evolution for a "pancake"-like injection with a sharp peak at $\mu = 0$. We also reduce the diffusion coefficient to $D_0 = 0.003$ to illustrate the effect of weak diffusion. We find that particles are generally not able to reach the escape cone even after about five crossing times. Their effective crossing and residence time is significantly prolonged due to the combination of the initial condition being far away from the loss cone and the weak diffusion.

4. Results and Discussion

To study the expected behavior of the escape time based on the kinetic equations, and to test the validity of the above equation, we have carried out simulations with $N = 10{,}000$ particles with different values for D_0 and η and for the three initial pitch-angle distributions (isotropic, pancake, beam). Figure 2 summarizes the results in three panels for the three initial conditions.

The left panel shows the case of isotropic injection, which as expected shows the best overall agreement between the simulation results (symbols) and the analytic expression given by Equation (2) for all three different convergence parameters η. Note that in the strong diffusion regime, the numerical results converge to the random walk expression $T_{\rm esc} \sim \tau_{\rm cross}^2/\tau_{\rm sc}$ independent of η and isotropy. However, there are significant deviations from this in the intermediate regime (starting at lower values of $\tau_{\rm sc}/\tau_{\rm cross}$ for larger η). For weak diffusion, the $\eta = 1$ case shows the free escape of particles, while the other two cases exhibit the $T_{\rm esc} \propto \tau_{\rm sc}$ behavior that is reproduced well by the simulations.

The middle panel shows the result for a beam injection of particles. With the forward SDE numerical scheme used here, we can inject particles at exactly $\mu = \pm 1$, resembling a very narrow bidirectional beam. The universal behavior in the strong diffusion regime is reproduced again, while the analytic expression breaks down in the weak diffusion regime, with all cases eventually converging to the crossing time. This happens at larger scattering times for higher η cases with smaller loss cones, $\theta_{\rm lcone} \sim 1/\sqrt{\eta}$. This can easily be explained by the fact that at shorter scattering times, particles initially in the loss cone are scattered out of it and remain in the site for a longer time for higher values of η.

Finally, in the right panel, we find that an initially strongly peaked pitch-angle distribution near $\mu = 0$ (pancake) shows overall similar behavior, but as expected slightly larger values for the escape time than in the isotropic injection case. The most notable difference in the weak diffusion regime for $\eta = 1$ can be explained due to the difficulty of scattering of particles from their initial large pitch angles ($\mu = 0$) to small angles at longer and longer scattering times.

5. Summary and Conclusions

In this Letter, we investigated the particle confinement and escape resulting from the interplay of isotropic turbulent pitch-angle scattering and magnetic field convergence. We compared numerical solutions for the relation between scattering and escape time calculated with an SDE scheme for the particle transport equation with an analytical approximation formula, based on the work of Malyshkin & Kulsrud (2001). We found good agreement between the approximation and the simulation results, but also notable differences in the weak diffusion regime that depend both on the initial pitch-angle distribution of particles and the field convergence rate represented by the mirror ratio η or scale height h_B.

The investigation of the acceleration and transport of particles in magnetized plasmas depends crucially on the escape time, because in most situations we do not observe the particles at the acceleration site. Instead, we observe the particles that have escaped the acceleration site and reached the near Earth instruments as CRs and SEPs, or indirectly through the radiation that they produce often away from the acceleration sites.

In some sources and under favorable observational situations, it is possible to measure the escape time and its energy dependence (see, e.g., Chen & Petrosian 2013; Petrosian & Chen 2014). The relation that we have established here can be used in such situations to determine the scattering time or the pitch-angle diffusion coefficient and hence provide information on acceleration and transport mechanisms. Expansion of these results to a more realistic situation that includes anisotropic

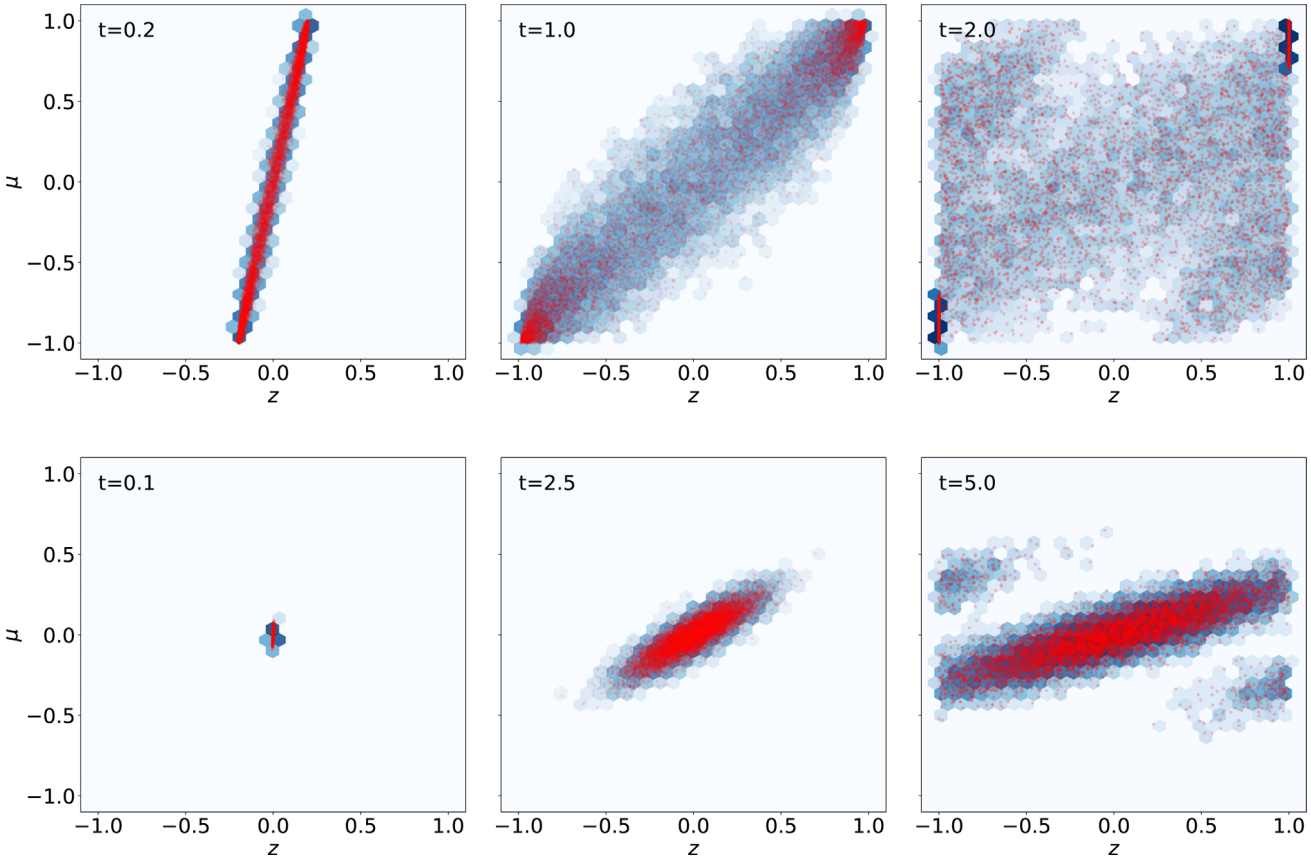

Figure 1. Pseudo-particle distribution in $z - \mu$ phase space for isotropic (upper panel) and "pancake" (lower panel) injection at three times during the evolution with $\eta = 2$ and $D_0 = 0.1$, or $\tau_{sc} = 5L/v$, (upper panel) and $D_0 = 0.003$ (lower panel). The red circles indicate individual particles and the blue background coloring is given by a hexagonal binning with arbitrary units (darker blue means more particles).

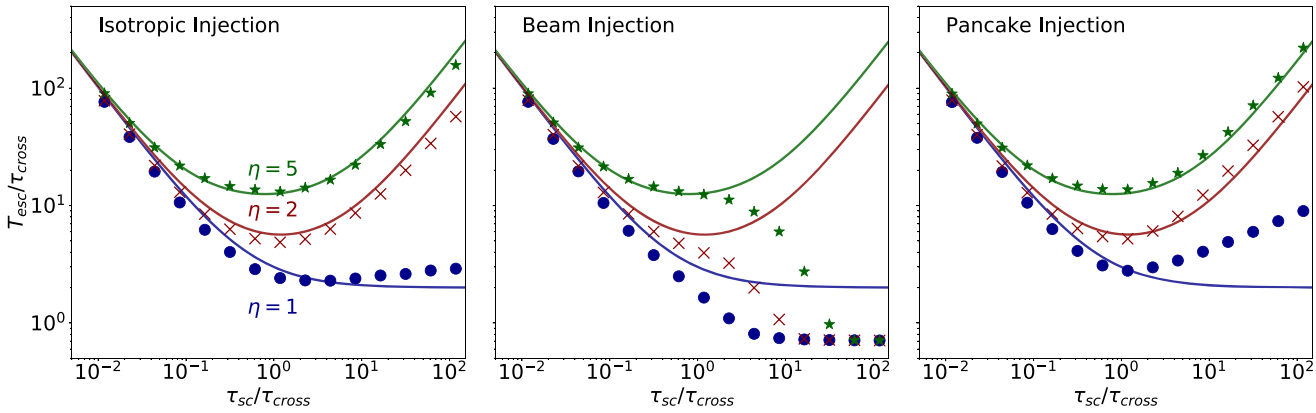

Figure 2. Particle escape times vs. scattering time τ_{sc} for three different values of mirror strength: $\eta_1 = 1$ (blue), $\eta_2 = 2$ (red), and $\eta_3 = 4$ (green) and three different injection functions. Symbols are from our simulations and solid lines are based on the analytic approximation of Equation (2).

pitch-angle diffusion coefficients and the dependence on energy of the processes discussed here can shed light on additional effects and the other important diffusion coefficient, namely energy or momentum diffusion, that plays an equally significant role in acceleration and transport processes. These aspects will be addressed in our future work.

This work was partially supported by NASA grants NNX14AG03G and NNX17AK25G. We acknowledge helpful discussions with J. McTiernan and N. Jeffrey and support from the International Space Science Institute through the ISSI team on "Solar flare acceleration signatures and their connection to solar energetic particles."

ORCID iDs

Frederic Effenberger https://orcid.org/0000-0002-7388-6581
Vahé Petrosian https://orcid.org/0000-0002-2670-8942

References

Achterberg, A., & Schure, K. M. 2011, MNRAS, 411, 2628
Ackermann, M., Allafort, A., Baldini, L., et al. 2017, ApJ, 835, 219

Ajello, M., Albert, A., Allafort, A., et al. 2014, ApJ, 789, 20
Armstrong, C. K., Litvinenko, Y. E., & Craig, I. J. D. 2012, ApJ, 757, 165
Bian, N. H., Emslie, A. G., Stackhouse, D. J., & Kontar, E. P. 2014, ApJ, 796, 142
Chalov, S. V., & Fahr, H. J. 1998, A&A, 335, 746
Chen, Q., & Petrosian, V. 2013, ApJ, 777, 33
Dröge, W., Kartavykh, Y. Y., Klecker, B., & Kovaltsov, G. A. 2010, ApJ, 709, 912
Dung, R., & Petrosian, V. 1994, ApJ, 421, 550
Earl, J. A. 1981, ApJ, 251, 739
Effenberger, F., Fichtner, H., Scherer, K., et al. 2012, ApJ, 750, 108
Effenberger, F., & Litvinenko, Y. E. 2014, ApJ, 783, 15
Effenberger, F., Rubio da Costa, F., Oka, M., et al. 2017, ApJ, 835, 124
Effenberger, F., Rubio da Costa, F., & Petrosian, V. 2016, Journal of Physics Conference Series, 767, 012005
Fichtner, H., Le Roux, J. A., Mall, U., & Rucinski, D. 1996, A&A, 314, 650
Fletcher, L. 1995, A&A, 303, L9
Fletcher, L., & Martens, P. C. H. 1998, ApJ, 505, 418
Gardiner, C. W. 2009, Stochastic Methods: A Handbook for the Natural and Social Sciences (Berlin: Springer)
Jeffrey, N. L. S., Kontar, E. P., Bian, N. H., & Emslie, A. G. 2014, ApJ, 787, 86
Jin, M., Petrosian, V., Liu, W., et al. 2018, ApJ, 867, 122
Kašparová, J., & Karlický, M. 2009, A&A, 497, L13
Kloeden, P., & Platen, E. 1995, Numerical Methods for Stochastic Differential Equations (Berlin: Spinger)
Kontar, E. P., Bian, N. H., Emslie, A. G., & Vilmer, N. 2014, ApJ, 780, 176
Kontar, E. P., Jeffrey, N. L. S., Emslie, A. G., & Bian, N. H. 2015, ApJ, 809, 35
Kopp, A., Büsching, I., Strauss, R. D., & Potgieter, M. S. 2012, CoPhC, 183, 530
Krucker, S., Hudson, H. S., Glesener, L., et al. 2010, ApJ, 714, 1108
Krucker, S., & Lin, R. P. 2008, ApJ, 673, 1181
Krucker, S., White, S. M., & Lin, R. P. 2007, ApJL, 669, L49
Leach, J., & Petrosian, V. 1981, ApJ, 251, 781
Leach, J., & Petrosian, V. 1983, ApJ, 269, 715
Lin, R. P., Dennis, B. R., Hurford, G. J., et al. 2002, SoPh, 210, 3
Litvinenko, Y. E., & Noble, P. L. 2013, ApJ, 765, 31
Liu, W., Chen, Q., & Petrosian, V. 2013, ApJ, 767, 168
Liu, W., Liu, S., Jiang, Y. W., & Petrosian, V. 2006, ApJ, 649, 1124
Liu, W., Petrosian, V., Dennis, B. R., & Jiang, Y. W. 2008, ApJ, 676, 704
MacKinnon, A. L., & Craig, I. J. D. 1991, A&A, 251, 693
Malyshkin, L., & Kulsrud, R. 2001, ApJ, 549, 402
Masuda, S., Kosugi, T., Hara, H., Tsuneta, S., & Ogawara, Y. 1994, Natur, 371, 495
McTiernan, J. M., & Petrosian, V. 1991, ApJ, 379, 381
Moravec, Z., Varady, M., Kašparová, J., & Kramoliš, D. 2016, AN, 337, 1020
Oka, M., Birn, J., Battaglia, M., et al. 2018, SSRv, 214, 82
Oka, M., Ishikawa, S., Saint-Hilaire, P., Krucker, S., & Lin, R. P. 2013, ApJ, 764, 6
Oka, M., Krucker, S., Hudson, H. S., & Saint-Hilaire, P. 2015, ApJ, 799, 129
Pesce-Rollins, M., Omodei, N., Petrosian, V., et al. 2015, ApJL, 805, L15
Petrosian, V. 2012, SSRv, 173, 535
Petrosian, V. 2016, ApJ, 830, 28
Petrosian, V., & Chen, Q. 2010, ApJL, 712, L131
Petrosian, V., & Chen, Q. 2014, PhRvD, 89, 103007
Petrosian, V., & Donaghy, T. Q. 1999, ApJ, 527, 945
Petrosian, V., Donaghy, T. Q., & McTiernan, J. M. 2002, ApJ, 569, 459
Petrosian, V., & East, W. E. 2008, ApJ, 682, 175
Petrosian, V., & Kang, B. 2015, ApJ, 813, 5
Petrosian, V., & Liu, S. 2004, ApJ, 610, 550
Piana, M., Massone, A. M., Hurford, G. J., et al. 2007, ApJ, 665, 846
Roelof, E. C. 1969, in Lectures in High-Energy Astrophysics, ed. H. Ögelman & J. R. Wayland (Washington, DC: NASA), 111
Schlickeiser, R. 1989, ApJ, 336, 243
Schlickeiser, R., & Shalchi, A. 2008, ApJ, 686, 292
Strauss, R. D., Potgieter, M. S., Büsching, I., & Kopp, A. 2011, ApJ, 735, 83
Strauss, R. D. T., & Effenberger, F. 2017, SSRv, 212, 151
Zuo, P., Zhang, M., Gamayunov, K., Rassoul, H., & Luo, X. 2011, ApJ, 738, 168